PCCP

PAPER

View Article Online
View Journal | View Issue

Cite this: *Phys. Chem. Chem. Phys.*, 2026, **28**, 3490

Bare group 10 metal atoms as vertices in polyhedral metallaboranes: spherical aromaticity in the icosahedral $MB_{11}H_{11}$ systems

Amr A. A. Attia,[a] Alexandru Lupan *[a] and R. Bruce King *[b]

The $MB_{n-1}H_{n-1}$ (M = Ni, Pd, Pt; n = 5 to 14) clusters with bare group 10 metal vertices have been examined by density functional theory. The lowest energy structures are found to be the corresponding *closo* deltahedra. This suggests that the group 10 metal atom can serve as four skeletal electron donors thereby providing the $2n + 2$ skeletal electrons for these *closo* systems in accord with the Wade–Mingos rules. A molecular orbital analysis of the icosahedral $NiB_{11}H_{11}$ suggests interpretation as a spherical aromatic system with 32 core electrons in a filled $1S^2 1P^6 1D^{10} 1F^{14}$ shell, analogous to superatomic 3D aromatic species. The molecular orbital analysis indicates that the valence s and d orbitals (mainly d_z^2) of the metal participate in delocalized bonding with the boron cage, while the remaining d-electrons reside in non-bonding orbitals localized on the metal. The result is a closed-shell, diamagnetic cluster with substantial aromatic stabilization. Comparisons between Ni, Pd, and Pt reveal similar structural trends, with the Ni-based clusters generally showing the largest stabilization of the *closo* form. The absence of any protective ligands in these clusters means that the metal centers are coordinatively unsaturated. However, the pronounced stability owing to delocalized skeletal bonding suggests that if isolated, such species would be resilient icosahedral clusters. This theoretical study provides a systematic baseline for bare metal metallaborane clusters, highlighting their viability and unique electronic structure (spherical aromaticity), while also noting the potential (yet untested) reactivity of an exposed transition-metal vertex.

Received 25th October 2025,
Accepted 12th January 2026

DOI: 10.1039/d5cp04106f

rsc.li/pccp

1. Introduction

Hawthorne and co-workers[1] discovered in the 1960s that the boron vertices in deltahedral boranes and isoelectronic carboranes could be replaced by transition metal vertices. The original 10 to 12 vertex metalladicarbaboranes synthesized by the Hawthorne group using decaborane, $B_{10}H_{14}$ as the boron source and alkynes as the carbon source were supplemented by smaller metallaboranes synthesized by Grimes and co-workers[2] using pentaborane, B_5H_9, as the boron source. The external coordination sites of the metal vertices in the metallaboranes initially prepared by Hawthorne, Grimes, and their coworkers and later by a number of other research groups were always protected by suitable external groups. The cyclopentadienyl (Cp) ligand was especially useful for this purpose because of its robust bonds formed with transition metals. Thus polyhedral metallaborane derivatives with CpM vertices can withstand relatively vigorous reaction conditions before rupture of the Cp–M bond leading to destruction of the metallaborane cluster. In this connection a CpCo unit was a vertex in many of the initially discovered metallaboranes since it is isolobal with a BH vertex. Many of the polyhedral metallaboranes synthesized later had other external groups such as arenes, carbonyl, nitrosyl, and/or phosphine ligands bonded to each of the transition metal vertices.

The originally synthesized metallaboranes and metallacarboranes had skeletons based on the most spherical *closo* deltahedra, which are characterized by vertices as nearly similar as possible and exclusively triangular faces (Fig. 1).[3,4] Thus the *closo* deltahedra having 6 to 12 vertices have only degree 4 and/or 5 vertices except for the 11-vertex deltahedron, which is topologically required to have a single degree 6 vertex. The number of skeletal electrons in such structures is generally determined by the Wade–Mingos rules,[5–7] which state that n-vertex *closo* deltahedral boranes are particularly stable if they contain $2n + 2$ skeletal electrons. This special stability has been ascribed to three-dimensional aromaticity.[8–10] In accord with the Wade–Mingos rules the so-called *closo* borane anions $B_nH_n^{2-}$ as well as the isoelectronic *closo* carboranes $CB_{n-1}H_n^-$

[a] *Faculty of Chemistry and Chemical Engineering, Babeş-Bolyai University, Cluj-Napoca, Romania. E-mail: alexandru.lupan@ubbcluj.ro*
[b] *Department of Chemistry, University of Georgia, Athens, 30602, Georgia. E-mail: rbking@uga.edu*

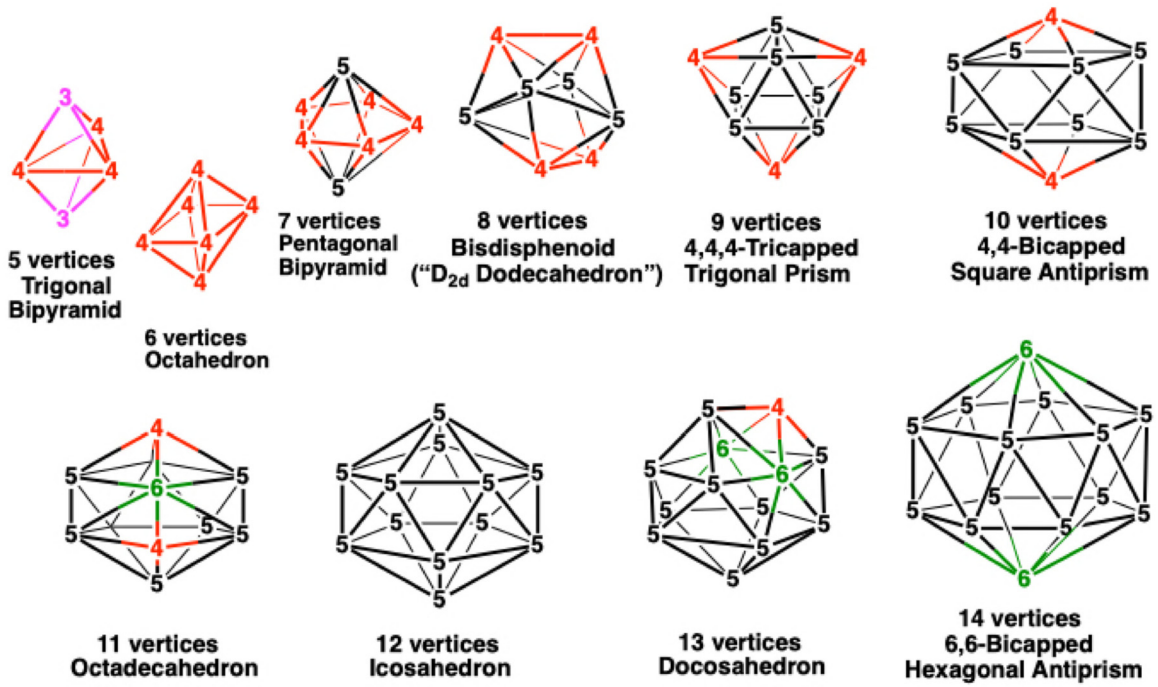

Fig. 1 The most spherical deltahedra with 5 to 12 vertices with the vertices labeled with their degrees. In addition, degree 3, 4, 5, and 6 vertices are shown in pink, red, black, and green, respectively.

and $C_2B_{n-2}H_n$ exhibit special stability. Much later work has led to the discovery of metal-free supraicosahedral metallaboranes such as the 13-vertex carboranes[11,12] 1,2μ-$C_6H_4(CH_2)_2$-3-C_6H_5-1,2-$C_2B_{11}H_{10}$ and 1,2-μ-$(CH_2)_3$-3-C_6H_5-1,2-$C_2B_{11}H_{10}$ by Xie and co-workers as well as the 14-vertex carborane (μ-$CH_2)_3C_2B_{12}H_{12}$.

A question of interest is whether polyhedral metallaboranes with bare transition metal vertices are accessible as viable species. If so, these clusters would feature chemically exposed metal sites that could, in principle, interact with other molecules allowing the designing clusters with novel reactivity or catalytic properties. Recent theoretical work by Merino and coworkers[13] provided a striking example: the $B_{10}Rh_2$ and $B_{10}Ir_2$ clusters were predicted as stable 12-vertex icosahedral structures, where two metal atoms occupy vertex positions in a framework otherwise consisting exclusively of boron atoms. These are described as *boron-based icosahedral clusters* stabilized by electron donation and covalent interactions from the metal atoms. Those findings support the idea that metal atoms can indeed stabilize *closo* boron clusters even without a full complement of ligands, essentially acting as electron-rich vertices that complete the cluster electron count.

Isolating a ligand-free metallaborane is challenging: without the stabilizing ligand, the metal center might either coordinate adventitiously to any available molecule or cause the cluster to rearrange. However, no such species have been synthesized or even characterized as reactive intermediates. In an attempt to predict the scope of such chemistry of this type we undertook a theoretical study of $MB_{n-1}H_{n-1}$ (M = Ni, Pd, Pt) derivatives using well-established density functional methods. The Group 10 metals were chosen for this initial study for the following reasons:

(1) They have the maximum number of valence electrons for transition metals likely to occur as vertex atoms.

(2) Reagents such as $Ni(CO)_4$, ($\eta^{5,5}$-$C_8H_{12})_1$Ni, ($\eta^{2,2,2}$-*cyclo*-1,5,9-$C_{12}H_{18}$)Ni, and $(C_2H_4)_3$Pt are available that can generate reactive "naked" metal atoms for reactions with boranes such as decaborane $B_{10}H_{14}$.

The $MB_{11}H_{11}$ (M = Ni, Pd, and Pt) systems included in this study are related to the icosahedral M_2B_{10} (M = Rh, Ir) systems studied by Merino and co-workers.[13] Other bare metal-boron clusters have been proposed for hydrogen storage.[14] The $MB_{11}H_{11}$ (M = Ni, Pd, and Pt) systems are examples of possible intermediates in such hydrogen storage processes.

The computational studies reported here by standard density functional methods indicate a strong preference for the most spherical *closo* deltahedral structures for these $B_{n-1}H_{n-1}M$ (M = Ni, Pd, Pt) systems. This suggests that each group 10 metal vertex Ni, Pd, and Pt is a donor of four skeletal electrons in order to provide such *n*-vertex *closo* deltahedral structures with the preferred $2n + 2$ skeletal electrons suggested by the Wade–Mingos rules.[5–7] Details of these studies are presented in this paper.

2. Theoretical methods

The initial chemical structures investigated in this study are based on various $B_nH_n^{2-}$ polyhedral frameworks (including all *closo* deltahedra from 5 to 14 vertices, and some other

structures) where a systematic substitution of one BH vertex led to the generation of 204 different starting structures of the type $MB_{n-1}H_{n-1}$ (M = Ni, Pd, Pt; n = 5 to 14) (see the SI).

Full geometry optimizations were carried out using the PBE0 DFT functional and the triple zeta def2-TZVP basis set for all atoms except for Pd and Pt for which the SDD (Stuttgart–Dresden ECP plus DZ) basis set was used. Single point energy calculations were performed on the lowest energy structures by employing the DLPNO-CCSD(T) method[15–28] coupled with the def2-QZVP//SDD basis set. Zero-point and thermal corrections taken from the PBE0/(def2-TZVP//SDD) computations were added to the final energies.

The nature of the stationary points was characterized by harmonic vibrational frequencies. When significant imaginary frequencies were encountered, the optimization was continued by following the normal modes corresponding to imaginary frequencies to ensure that genuine minima were obtained. All of the low-energy structures have substantial HOMO–LUMO gaps (see the SI). Electronic structures were analyzed by examining Kohn–Sham molecular orbitals, natural population analysis (NPA) charges, and the electron density distribution. We paid special attention to the symmetry and composition of the frontier orbitals to identify patterns consistent with spherical shell models. The adaptive natural density partitioning (AdNDP) method was not explicitly performed in this work, but we refer to literature AdNDP results on related boron clusters[29] for interpreting our bonding findings.

All calculations were performed using the Gaussian 09 package[30] with the default settings for the SCF cycles and geometry optimizations. Single-point DLPNO-CCSD(T) energy calculations were carried out with the ORCA 3.0.3 software package[31–39] using very tight convergence criteria.

The $MB_{n-1}H_{n-1}$ (M = Ni, Pd, Pt; n = 5 to 14) structures are designated as **B(n−1)M-x** where n is the total number of

Table 1 Optimized structures for the $B_{n-1}H_{n-1}M$ (M = Ni, Pd, Pt) systems with the stars indicating the degree of the metal vertex

Structure (symmetry)	ΔE (kcal mol^{-1})			Vertex degrees				Comments
	M = Ni	M = Pd	M = Pt	v_3	v_4	v_5	v_6	
5 vertices								
B4M-1 (C_{3v})	0.0	0.0	0.0	2*	3	0	0	Trigonal bipyramid
B4M-2 (C_s)	6.5	3.4	13.4	2	3*	0	0	Trigonal bipyramid (μ-H)
6 vertices								
B5M-1 (C_{4v})	0.0	0.0	0.0	0	6*	0	0	Octahedron
B5M-2 (C_1)	32.4	37.8	31.5	2*	2	2	0	Bicapped tetrahedron
7 vertices								
B6M-1 (C_{2v})	0.0	0.0	0.0	0	5*	2	0	Pentagonal bipyramid
B6M-2 (C_{5v})	21.6	15.7	12.5	0	5	2*	0	Pentagonal bipyramid
8 vertices								
B7M-1 (C_s)	0.0	0.0	0.0	0	4*	4	0	Bisdisphenoid
B7M-2 (C_1)	17.0	11.7	16.2	2*	0	5	0	Bicapped octahedron
9 vertices								
B8M-1 (C_{2v})	0.0	0.0	1.8	0	3*	6	0	Tricapped trigonal prism
B8M-2 (C_1)	11.2	5.8	0.0	0	3	6*	0	Tricapped trigonal prism
10 vertices								
B9M-1 (C_{4v})	0.0	0.0	0.0	0	2*	8	0	Bicap tetragonal antiprism
B9M-2 (C_s)	14.6	10.2	5.3	0	2	8*	0	Bicap tetragonal antiprism
11 vertices								
B10M-1 (C_s)	0.0	0.0	0.0	0	2*	8	1	11-vertex *closo* deltahedron
B10M-2 (C_1)	6.6	3.6	4.3	0	2	8	1*	11-v *closo* deltahed (distorted)
B10M-3 (C_s)	19.9	24.5	16.5	0	2	8	1*	11-vertex *closo* deltahedron
B10M-4 (C_s)	23.3	17.0	17.8	0	2	8*	1	11-vertex *closo* deltahedron
12 vertices								
B11M-1 (C_{5v})	0.0	0.0	0.0	0	0	12*	0	Icosahedron
B11M-2 (C_s)	44.6	51.4	42.3	0	2	8	2*	$2v_6$ deltahedron
13 vertices								
B12M-1 (C_{2v})	0.0	1.0	10.8	0	1*	10	2	13-vertex *closo* deltahedron
B12M-2 (C_s)	6.4	0.0	0.0	0	1	10*	2	13-vertex *closo* deltahedron
B12M-3 (C_s)	23.9	15.4	16.5	0	1	10*	2	13-vertex *closo* deltahedron
14 vertices								
B13M-1 (C_s)	0.0	2.2	0.0	0	0	12*	2	Bicapped hexagonal antiprism
B13M-2 (C_{3v})	6.4	0.0	25.1	2*	0	6	6	Bicapped icosahedron
B13M-3 (D_{6d})	18.7	13.0	4.6	0	0	12	2*	Bicapped hexagonal antiprism

polyhedral vertices, and x is the relative order of the structure on the potential energy scale. Only the lowest energy and thus potentially chemically significant structures are considered in detail in this paper. More comprehensive structural information, including higher energy structures and connectivity information not readily seen in the figures, are given in the SI.

The optimized structures for the $B_{n-1}H_{n-1}M$ (M = Ni, Pd, Pt) systems are listed in Table 1. The degrees of the metal vertices are starred. Except for the 11-vertex $MB_{10}H_{10}$ systems the figures depict the structures of the palladium derivatives as examples of similar derivatives of all three metals.

3. Results

The two lowest energy five-vertex MB_4H_4 (M = Ni, Pd, Pt) structures have a central MB_4 trigonal bipyramid corresponding to the *closo* 5-vertex deltahedron (Fig. 2 and Table 1). Among the two possible such structures the C_{3v} structures **B4M-1** with the metal atom M located at a degree 3 axial vertex is the lower energy structure. The other trigonal bipyramidal MB_4H_4 structures, namely the C_s structures **B4M2** with the metal atom located at a degree 4 equatorial vertex, lie 3.4 kcal mol^{-1} (M = Pd) to 13.4 kcal mol^{-1} (M = Pt) in energy above the corresponding **B4M-1** structure. In the **B4M2** structures one of the hydrogen atoms bridges an edge from an axial degree 3 boron vertex to an equatorial degree 4 vertex.

The lowest energy six-vertex MB_5H_5 (M = Ni, Pd, Pt) structures **B5M-1** have a central MB_5 octahedron corresponding to the *closo* 6-vertex deltahedron (Fig. 3 and Table 1). These C_{4v} structures appear to be very favorable since the next lower energy MB_5H_5 structures **B5M-2** lie 31.5 kcal mol^{-1} (M = Pt) to 37.8 kcal mol^{-1} (M = Pd) in energy above **B5M-1**. The **B5M-2** structures have a central MB_5 bicapped tetrahedron with the metal atom located at a degree 3 vertex.

The two lowest energy seven-vertex MB_6H_6 structures have central MB_6 pentagonal bipyramids corresponding to the *closo* 7-vertex deltahedron (Fig. 4 and Table 1). Among these structures the lower energy structures **B6M-1** are C_{2v} structures with the metal atom located at a degree 4 equatorial vertex. The higher energy C_{5v} structures **B6M-2**, lying 12.5 kcal mol^{-1} (M = Pt) to 21.6 kcal mol^{-1} (M = Ni) above the corresponding **B6M-1** structure (Table 1), have the metal atoms located at a degree 5 axial vertex.

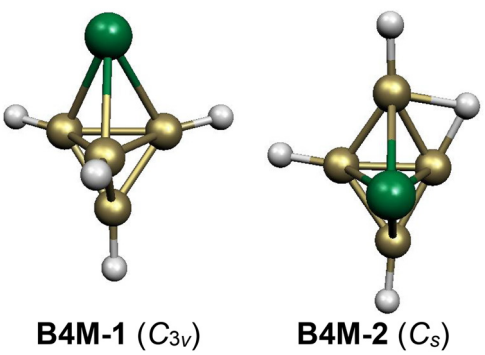

Fig. 2 The lowest energy five-vertex MB_4H_4 (M = Ni, Pd, Pt) structures.

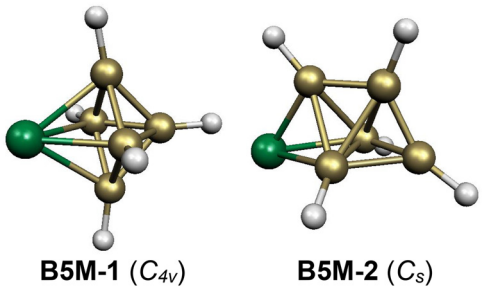

Fig. 3 The lowest energy six-vertex MB_5H_5 (M = Ni, Pd, Pt) structures.

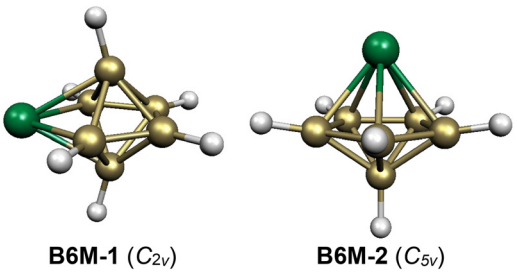

Fig. 4 The lowest energy seven-vertex MB_6H_6 (M = Ni, Pd, Pt) structures.

The lowest energy eight-vertex MB_7H_7 structures **B7M-1** have central bisdisphenoids corresponding to the *closo* 8-vertex deltahedron (Fig. 1) with the metal atoms located at a degree 4 vertex (Fig. 5 and Table 1). The next lowest energy MB_7H_7 structures **B7M-2** are C_{3v} bicapped octahedral structures with the metal atom at one of the degree 3 vertices. Structures **B7M-2** lie from 11.7 kcal mol^{-1} (M = Pd) to 17.0 kcal mol^{-1} (M = Ni) in energy above the corresponding **B7M-1** structures.

The two lowest energy nine-vertex MB_8H_8 (M = Ni, Pd, Pt) structures have a central MB_8 tricapped trigonal prism corresponding to the *closo* 9-vertex deltahedron (Fig. 6 and Table 1). The lowest energy structure **B8M-1** for the nickel and palladium MB_8H_8 derivatives has the metal atom located at a degree 4 vertex. The isomeric *closo* structure **B8M-2** with the metal located at a degree 5 vertex lies 11.2 kcal mol^{-1} (M = Ni) or 5.8 kcal mol^{-1} (M = Pd) above **B8M-1**. However, the *closo* structures **B8M-2** have an unusually long B–B edge between

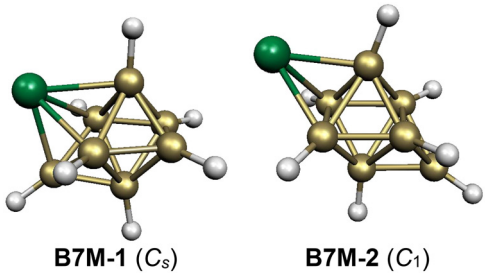

Fig. 5 The lowest energy eight-vertex MB_7H_7 (M = Ni, Pd, Pt) structures.

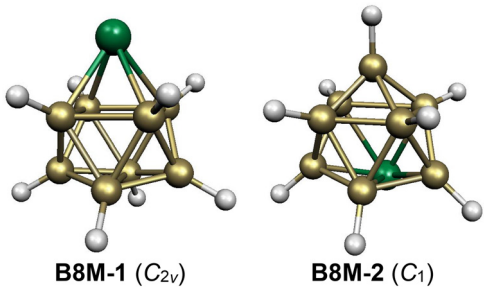

Fig. 6 The lowest energy nine-vertex MB_8H_8 (M = Ni, Pd, Pt) structures.

two of the boron atoms connected to the metal atom. The relative energy order of these two structure types is reversed for the platinum derivative PtB_8H_8 with **B8M-2** with the platinum atom at a degree 5 vertex lying 1.8 kcal mol^{-1} in energy below **B8M-1** with the platinum atom at a degree 4 vertex.

The two lowest energy ten-vertex MB_9H_9 (M = Ni, Pd, Pt) structures have central MB_9 bicapped square antiprisms corresponding to the *closo* 10-vertex deltahedron (Fig. 7 and Table 1). The lowest energy such structures **B9M-1** have C_{4v} symmetry with the metal atom located at one of the two degree 4 axial vertices. The higher energy such structures **B9M-2**, lying 5.3 kcal mol^{-1} (M = Pt) to 14.6 kcal mol^{-1} (M = Ni) above their lowest energy isomers, have the metal atom located at a degree 5 vertex.

The situation with the 11-vertex $MB_{10}H_{10}$ (M = Ni, Pd, Pt) systems is more complicated owing to the lower symmetry of the 11-vertex *closo* deltahedron which has one degree 6 vertex and eight degree 5 vertices as well as two degree 4 vertices flanking the unique degree 6 vertex (Fig. 1). Four fundamental types of $MB_{10}H_{10}$ structures are found within a reasonable energy range, all based on the 11-vertex *closo* deltahedron as illustrated in Fig. 8. The lowest energy **B10M-1** structures consistently have the metal atom at one of the two degree 4 vertices. Two types of $MB_{10}H_{10}$ structures are found with the metal atom at the unique degree 6 vertex. One of these structures, as exemplified by **B10Ni-3**, lying 19.9 kcal mol^{-1} in energy above **B10Ni-1**, has the nickel atom at the degree 6 vertex with all of its six bonds to adjacent boron atoms falling in the narrow range from 2.0 Å to 2.1 Å. However, distortion of the six Ni–B bonds from the degree 6 vertex so that two are elongated to 2.55 Å, two remain at 2.14 Å, and two are shortened to 1.84 Å leads to the much lower energy structure **B10Ni-2**, lying only 6.6 kcal mol^{-1} in energy above **B10Ni-1**. A similar distortion of the $MB_{10}H_{10}$ structure with the metal atom at the degree 6 vertex was found for both the platinum and the palladium systems. In the lowest energy $MB_{10}H_{10}$ structures with the metal atom at a degree 5 vertex, as exemplified by **B10Ni-4** lying 23.3 kcal mol^{-1} above **B10Ni-1**, the metal atom is located at the pseudo-antipodal degree 5 vertex relative to the unique degree 6 vertex.

For the 12-vertex $MB_{11}H_{11}$ (M = Ni, Pd, Pt) systems the unique icosahedral structures are by far the lowest energy structures (Fig. 9 and Table 1). Thus the lowest energy non-icosahedral $MB_{11}H_{11}$ isomers **B11M-2**, lie 42.3 kcal mol^{-1} (M = Pt) to 51.4 kcal mol^{-1} (M = Pd) in energy above **B11M-1**. These C_s **B11M-2** structures have two degree 4 and two degree 6 vertices with the metal atom located at one of the degree 6 vertices.

The $MB_{11}H_{11}$ (M = Pd, Pt) systems are related to the M_2B_{10} (M = Rh, Ir) systems studied by Merino and coworkers[13] with the bare group 9 rhodium and iridium vertices as donors of three skeletal electrons. They find icosahedral structures for

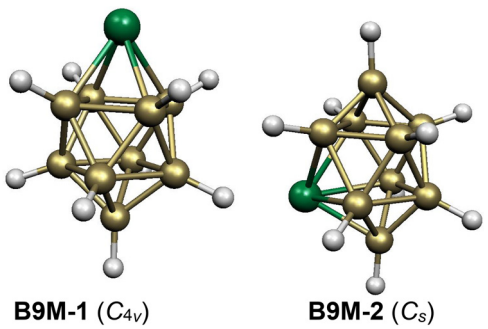

Fig. 7 The lowest energy ten-vertex MB_9H_9 (M = Ni, Pd, Pt) structures.

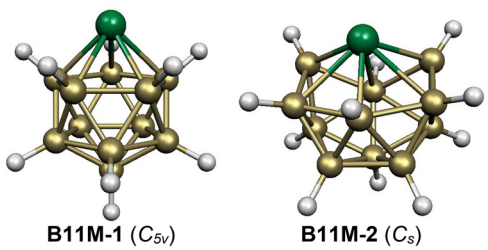

Fig. 9 The lowest energy 12-vertex $MB_{11}H_{11}$ (M = Ni, Pd, Pt) structures.

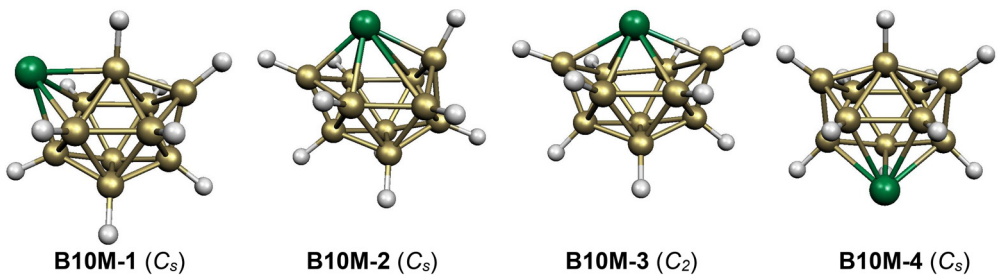

Fig. 8 The lowest energy 11-vertex $NiB_{10}H_{10}$ structures.

these M_2B_{10} derivatives with the two metals in antipodal (para) positions of the icosahedron to be the global minima lying 16.7 kcal mol^{-1} (M = Rh) and 18.0 kcal mol^{-1} (M = Ir) in energy below the next lowest energy structures.

The lowest-energy structures of the 13-vertex systems $MB_{12}H_{12}$ (M = Ni, Pd, Pt) are all based on the 13-vertex *closo* deltahedron, sometimes called the docosahedron because of its 22 faces (Fig. 1). The structure with the metal atom at a degree 5 vertex adjacent to both degree 6 vertices (**B12M-1** in Fig. 10) and the structure with the metal atom at the unique degree 4 vertex (**B12M-2** in Fig. 10) are the two lowest energy structures for all three metals. However, the relative energies of these two structures are highly dependent on the metal atom (Table 1). Thus these two structures are of similar energy within ~1 kcal mol^{-1} for palladium. However, for nickel the structure **B12Ni-2** with the nickel atom at the degree 4 vertex lies 6.4 kcal mol^{-1} in energy below **B12Ni-1** with the nickel atom at a degree 5 vertex connected to both degree 6 vertices. The reverse is found for platinum with an energy difference of 10.8 kcal mol^{-1}. Consistently higher in energy by margins ranging from 15.4 kcal mol^{-1} for palladium to 23.9 kcal mol^{-1} for nickel are next lowest energy structures with the metal atom at a degree 5 vertex connected to only one of the two degree 6 vertices.

The lowest energy structures for the 14-vertex $MB_{13}H_{13}$ (M = Ni, Pd, Pt) systems (Fig. 11) include structures based on the 14-vertex *closo* deltahedron, namely the bicapped hexagonal antiprism (Fig. 1) as well as the symmetrically bicapped icosahedron. The bicapped hexagonal antiprism structures **B13M-1** with the metal atom at one of the degree 5 vertices are the lowest energy structures for nickel and platinum and lie within 2 kcal mol^{-1} of the lowest-energy structure for palladium. The bicapped icosahedron structures **B13M-2** are the lowest energy structure for palladium, lie 6.4 kcal mol^{-1} above the lowest energy structure for nickel, but are a high-energy structure for platinum (Table 1). Conversely, the bicapped hexagonal antiprism structures **B13M-3** with the metal atom at one of the two degree 6 axial vertices lie only 4.6 kcal mol^{-1} above the lowest energy for platinum but are high-energy structures for nickel and palladium.

4. Discussion

4.1. Electronic structure and bonding analysis

Our theoretical studies show that structures based on *closo* deltahedra (Fig. 1) are clearly preferred energetically for all of the $MB_{n-1}H_{n-1}$ (M = Ni, Pd, Pt) systems having from 5 to 14 vertices thereby suggesting that these systems have $2n + 2$ skeletal electron based on the Wade–Mingos rules.[5–7] Since the BH vertices each provide two skeletal electrons, this means

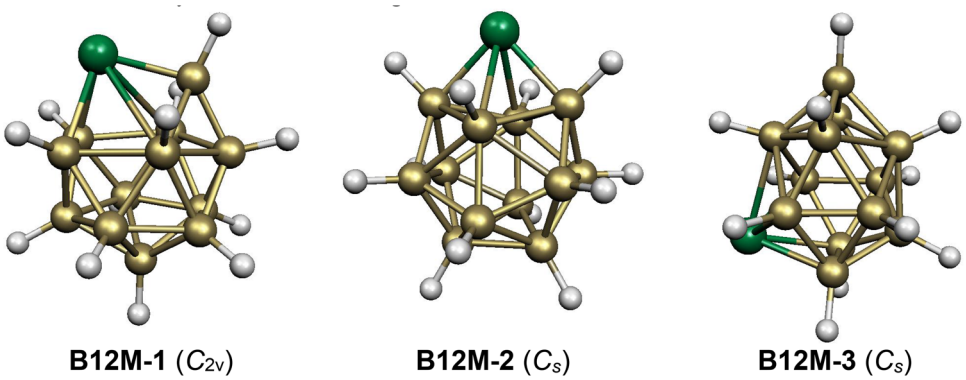

Fig. 10 The lowest energy 13-vertex $MB_{12}H_{12}$ (M = Ni, Pd, Pt) structures.

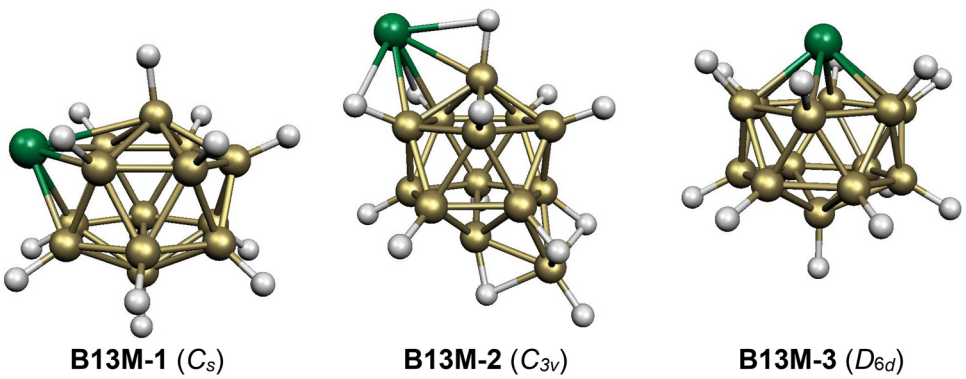

Fig. 11 The lowest energy 14-vertex $MB_{13}H_{13}$ (M = Ni, Pd, Pt) structures.

that a group 10 metal vertex (Ni, Pd, Pt) must provide four skeletal electrons. Thus the 10 valence electrons of the neutral group 10 metals are partitioned into four skeletal electrons and six external electrons. The six external electrons correspond to three external lone pairs in these singlet state structures.

The $MB_{n-1}H_{n-1}$ (M = Ni, Pd, Pt) systems also obey the $4m + 2$ interstitial electron rule of Jemmis and Schleyer[40] where $m = n + 1$. Thus the boron and hydrogen atoms of the $B_{n-1}H_{n-1}$ portion of the deltahedron contribute three and one interstitial electrons, respectively, resulting in $4(n - 1)$ interstitial electrons from this portion of the molecule. The group 10 transition metal atom (Ni, Pd, Pt) with a d^{10} configuration contributes an additional 10 electrons leading to a total of $4(n + 1) + 2 = 4m + 2$ interstitial electrons.

In the lowest energy structures of most of the $MB_{n-1}H_{n-1}$ (M = Ni, Pd, Pt) systems, the metal atom is located at a degree 4 vertex rather than a degree 5 vertex. Also, in the trigonal bipyramidal 5-vertex MB_4H_4 systems there is an energetic preference for the location of the metal atom at one of the two degree 3 axial vertices rather than at one of the three degree 4 equatorial vertices. The preferred location of the metal atom at degree 3 vertices is also indicated by structures with metals located at degree 3 vertex caps in bicapped octahedral structures **B7M-2** and bicapped icosahedral structures **B13M-2** for the 8- and 14-vertex systems, respectively, being energetically competitive with structures based on the corresponding *closo* deltahedra (Fig. 1), namely the 8-vertex bisdisphenoid and 14-vertex bicapped hexagonal antiprism.

Consider the graph theory derived model for the skeletal bonding in *closo* boranes and related structures.[9] Each vertex atom provides three internal orbitals for the skeletal bonding. One of these orbitals from each vertex atom in an *n*-vertex system, designated as an internal or radial orbital, overlaps with the corresponding orbitals from all of the other vertex atoms in the center of the deltahedron to form an *n*-center core bond requiring two skeletal electrons. The two other internal orbitals from each vertex atom overlap pairwise on the surface of the deltahedron thereby forming *n* two-center two-electron (2c–2e) bonds requiring $2n$ skeletal electrons. In this way the requirement of $2n + 2$ skeletal electrons for *closo* deltahedral structures can be rationalized. Furthermore, a set of *n* 2c–2e surface bonds can be considered as a canonical form of a resonance structure analogous to a Kekulé structure of benzene. Thus the totality of all possible such sets of *n* 2c–2e surface bonds provides a delocalized system corresponding to the three-dimensional aromaticity of such systems. This can account for the energetic preference of such *closo* deltahedral structures for these systems.

By inspecting the Kohn–Sham orbitals of, for instance, $NiB_{11}H_{11}$, we find that the 4s and 3d orbitals of the nickel atom mix into the delocalized bonding orbitals of the cluster. In the *closo* icosahedral cluster, the skeletal bonding MOs can be grouped by their symmetry as s-like, p-like, d-like, *etc.*, corresponding to spherical harmonics on the icosahedron. The nickel atom contributes significantly to a few of these. Thus the lowest s-like combination and one set of d-like combinations (analogous to d_z^2 oriented into the cluster) have noticeable Ni character (>50% localization on Ni in those MO lobes). These orbitals correspond to Ni using one s and approximately two of its five 3d orbitals in bonding (an sd^2 hybrid, so to speak). The remaining d orbitals (particularly those of E (x^2 y^2, xy) and T (xz, yz) symmetry on the icosahedron) do not find good overlap with cluster framework orbitals and end up essentially as Ni-centered lone pairs. This picture aligns with classical ideas of transition metal cluster bonding: not all metal d orbitals will engage in skeletal bonding, only those that that are allowed by symmetry and energy. Nickel uses roughly three valence orbitals (one 4s + two 3d) to form cluster bonds, leaving $3d^6$ worth of electrons essentially on the Ni (as non-bonding or core-like orbitals).

This description is supported by the AdNDP perspective reported for closo boranes:[29] in $B_{12}H_{12}^{2-}$, all 26 valence electrons can be classified into multi-center two-electron bonds spanning the cage (with varying degrees of delocalization: some 3-center B–B–B bonds, some 4-center, and an overall 12-center delocalized component). In $NiB_{11}H_{11}$, we expect a similar situation, except now there are 26 + 4 = 30 skeletal electrons (since the cluster is neutral, we actually have 24 from BH units + 4 from Ni = 28 skeletal bonding electrons by Wade–Mingos counting; plus 2 extra that might occupy a non-bonding or higher antibonding level). The presence of the metal does not localize the bonding into 2-center bonds; rather, it contributes to the delocalized bonds. If one performed an AdNDP, one might find a set of multi-center bonds that include the metal as one of the centers, reflecting Ni–B–B three-center bonds or Ni–B–B–B four-center bonds, *etc.*, alongside the multi-B bonds. The key point is that the bonding remains collective. For instance, the computed Wiberg bond indices (WBI) show that Ni has a non-negligible bond index with each of its neighboring B atoms ($\sim$0.3–0.4 per Ni–B in $NiB_{11}H_{11}$), summing to $\sim$1.6, which is close to Ni effectively forming the equivalent of a 2c–2e bond distributed over the cluster. This is very much in line with an *isolobal analogy*: Ni in $NiB_{11}H_{11}$ behaves like a 16-electron fragment donating into a boron cage, analogous to CoCp (18e) or $Fe(CO)_3$ (18e) in other contexts, except here Ni has no external ligands.

The $MB_{n-1}H_{n-1}$ (M = Ni, Pd, Pt) derivatives are clearly coordinatively unsaturated systems since the metal atoms formally use only a six-orbital sd^5 manifold leaving their three higher-energy p orbitals out of their chemical bonding manifold. The $MB_{n-1}H_{n-1}$ derivatives are thus expected to be highly reactive towards bonding of various ligands to the bare metal atom leading to $L_3MB_{n-1}H_{n-1}$ derivatives such as $(\eta^6\text{-}C_6H_6)MB_{n-1}H_{n-1}$ or $B_{n-1}H_{n-1}M(CO)_3$. In such structures the metal uses its full nine-orbital sp^3d^5 manifold with the favored 18-electron configuration and also retaining the favorable $2n + 2$ skeletal electrons of the central MB_{n-1} *closo* deltahedron. However, the viability of the bare metal atom *closo* deltahedral $MB_{n-1}H_{n-1}$ structures, as suggested by the calculations reported here, suggests that the binding of the ligands L attached to the metal atom in their $L_3MB_{n-1}H_{n-1}$ derivatives is likely to be relatively weak. As a result, the

$L_3MB_{n-1}H_{n-1}$ derivatives are predicted to be labile towards substitution reactions involving the ligands L.

The icosahedral $MB_{11}H_{11}$ (M = Ni, Pd, Pt) structures exhibit the highest symmetry (C_{5v}) of the $MB_{n-1}H_{n-1}$ (n = 5 to 12) structures investigated. They also appear to be the most stable of the $MB_{n-1}H_{n-1}$ structures as suggested by the thermochemistry of cluster buildup reactions of the type $MB_{n-1}H_{n-1}$ + BH → MB_nH_n which are all exothermic. Thus for n values from 6 to 10 such cluster buildup reactions liberate 95 to 121 kcal mol^{-1} for each step. However, the cluster buildup reactions from the 11-vertex $MB_{10}H_{10}$ to the 12-vertex $MB_{11}H_{11}$ are significantly more exothermic liberating ~135 kcal mol^{-1}. This suggests greater thermochemical stability of the 12-vertex system.

In order to provide more insight into the chemical bonding in these systems, we investigated the bonding molecular orbitals of the icosahedral nickel structure $NiB_{11}H_{11}$ **B11Ni-1** (Fig. 12). The 12-vertex system was chosen because of its greater symmetry as well as its apparent greater thermochemical stability. In $NiB_{11}H_{11}$ the single nickel atom, 11 boron atoms, and 11 hydrogen atoms have a total of 94 electrons, among which 40 are inner core electrons not involved in the chemical bonding and occupying the core molecular orbitals from 1 to 20. The remaining 54 valence electrons, consisting of 10 electrons from the nickel atom, 33 electrons from the 11 boron atoms, and 11 electrons from the 11 hydrogen atoms, occupy the 27 molecular orbitals from 21 to 47. These 54 valence electrons can be partitioned into 22 external electrons for the 11 external B–H bonds and 32 internal electrons for the bonding within the NiB_{11} cluster. Note that the 32 internal electrons include the 26 electrons for the skeletal bonding in the NiB_{11} icosahedron as well as 6 electrons for the three lone pairs in the three external nickel orbitals of its sd^5 manifold. Furthermore, 32 (= $2(N+1)^2$ for N = 3) electrons is a "magic number" for a filled $1S^21P^61D^{10}1F^{14}$ set of molecular orbitals in a spherical aromatic system.[41]

The nine lowest-energy bonding molecular orbitals from 21 to 29 can clearly be identified by their shapes as the $1S^21P^61D^{10}$ part of the internal bonding of the NiB_{11} core of **B11Ni-1** (Fig. 12). The remaining part of the internal core bonding, namely the $1F^{14}$ part, is not quite as clear but appears to corresponding to the molecular orbitals from 31 to 37. Molecular orbital 30, lying between the $1D^{10}$ and $1F^{14}$ parts of the cluster bonding, appears to relate to the B–H external bonding since it is located essentially completely on the B_{11} part of the central cluster. The remaining 10 bonding molecular orbitals in $NiB_{11}H_{11}$ from 38 to the HOMO (47) appear to arise mainly from the external B–H bonds with this being clearest for the molecular orbitals from 42 to 44 that, like molecular orbital 30, have little electron density on the nickel atom.

4.2. Stability and potential reactivity of bare-metal clusters

Our calculations firmly establish that, *in silico*, $MB_{n-1}H_{n-1}$ clusters (M = Ni, Pd, Pt) exhibit *closo* structures that are

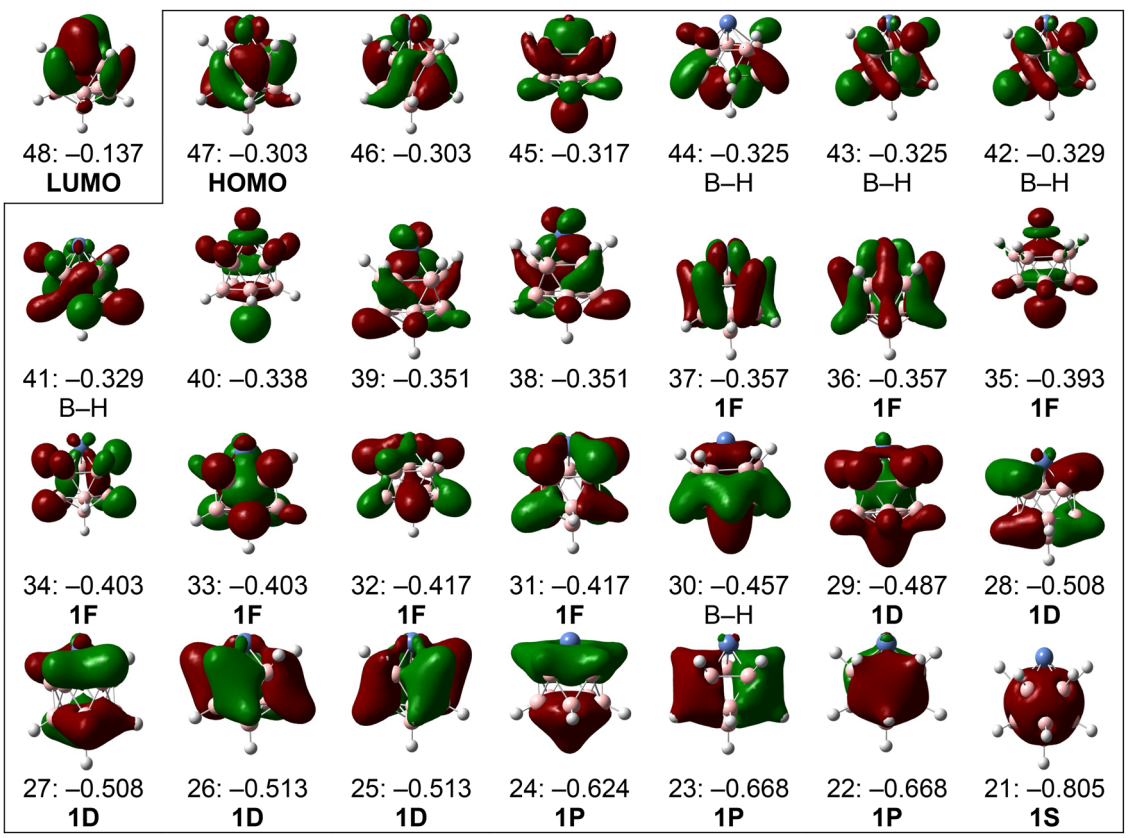

Fig. 12 Bonding molecular orbitals of the icosahedral $NiB_{11}H_{11}$ structure **B11Ni-1**. The orbitals in the $1S^21P^61D^{10}1F^{14}$ cluster bonding manifold are indicated in red and the B–H external orbitals are indicated in green. Orbital energies are given in atomic units.

particularly stable as compared to other cluster arrangements. The question of whether these clusters could be realized experimentally is connected with their *reactivity*. A naked metal center on a boron cage is a highly unusual coordination environment in which the metal is short of the favorable 18-electron count. In $NiB_{11}H_{11}$, Ni is necessarily located at a degree 5 vertex using 4 electrons for cluster bonding leaving 6 non-bonding electrons in external lone pairs thereby totalling 10 valence electrons, which is far below the favorable 18-electron configuration. Such an electronically unsaturated metal atom might be expected to strongly attract ligands or reactants to approach or achieve the favorable 18-electron configuration. On the other hand, the entire cluster is a closed-shell singlet with aromatic stabilization so addition of a ligand might disrupt the delicate electronic balance.

In order to evaluate this, the addition of simple ligands such as CO to the bare metal atom can be considered. For example, if $NiB_{11}H_{11}$ were exposed to CO, the Ni could in principle bind up to three CO molecules to make an 18-electron Ni(0) complex $Ni(CO)_3B_{11}H_{11}$. Such a reaction would be

$$NiB_{11}H_{11} + 3CO \rightarrow Ni(CO)_3B_{11}H_{11}$$

This reaction would require Ni to shift some electron density for bonding to CO ligands. Since CO is a strong field ligand; it would compete for the 3d and 4s electrons that Ni is currently sharing with the $B_{11}H_{11}$ cluster. Bonding of an external CO ligand to a Ni cluster vertex could require the Ni atom to withdraw some electron donation from the cage to satisfy the CO bonds. This might effectively reduce the skeletal electron count of the cage, possibly destabilizing the *closo* framework.

In essence, the cluster might need to sacrifice some aromatic stabilization to let Ni achieve a favorable 18-electron configuration. Which effect wins out depends on energetics: Ni–CO bonds are worth on the order of 30–40 kcal mol^{-1} each in typical complexes, whereas the aromatic stabilization of $NiB_{11}H_{11}$ (going from an open structure to *closo*) is $\sim$50 kcal or more (the gap we saw to alternatives). It is plausible that $NiB_{11}H_{11}$ doesn't gain much (or even loses) by binding external CO groups. Our reasoning supports that the cluster is already electronically satisfied, so adding external ligands diminishing returns. Thus if ligands coordinate, their binding might be only be moderate to preserve an intact *closo* cage.

From another angle, consider chemical reactivity such as oxidative addition or insertion at the metal. A bare Ni(0) site is normally very reactive as shown by Ni(0) organometallics activating C–H bonds. However, in $NiB_{11}H_{11}$ the Ni(0) is part of an aromatic cage. Thus any reaction that changes electron count will affect the electron count of the entire cage. For instance, oxidative addition to $NiB_{11}H_{11}$ would formally give something like H–Ni–H bonded to $B_{11}H_{11}$, thereby disrupting the *closo* system. (This could lead to a *nido* or *arachno* structure with an open face to accommodate Ni(II).) Thus these clusters likely sit in a delicate balance by being *kinetically inert because of the aromatic cage*, but *thermodynamically open to reaction* because the metal has unused capacity.

No experimental data are currently available to provide a direct comparison with our theoretical results. However, such clusters might be generated by a transient route such as removal of the CO ligands from a $Ni(CO)_3B_{11}H_{11}$ complex leading to $NiB_{11}H_{11}$ in the gas phase for observation by mass spectrometry. The inherent stability of $NiB_{11}H_{11}$ favors its existence long enough to detect. The high negative charge on the boron atoms and the positive change on the Ni atom might make $NiB_{11}H_1i$ subject to electrophilic attack at boron or nucleophilic attack at Ni.

In summary, these bare-metal *closo* clusters are likely quite *inert to cluster fragmentation* owing to strong delocalized bonding so they will not easily undergo dehydrogenation or even fall apart. They are also electron-rich yet coordinatively unsaturated at the metal, so they might form adducts or undergo addition reactions at the metal. However, in doing they compromise their spherical aromaticity. Any practical catalytic application would require a mechanism to harness the reactivity of the metal atom while keeping the cage intact. This could lead to use of the cluster as a bound ligand itself, thereby entering the realm of supraicosahedral chemistry rather than classical catalysis.

5. Summary

The lowest energy structures for the $MB_{n-1}H_{n-1}$ (M = Ni, Pd, Pt; n = 5 to 14) clusters with bare group 10 metal vertices are the corresponding *closo* deltahedra. This suggests that the group 10 metal vertices use a 6-orbital sd^5 manifold to become donors of 4 skeletal electrons thereby providing the $2n + 2$ skeletal electrons for these *closo* systems in accord with the Wade–Mingos rules. A molecular orbital analysis of the icosahedral $NiB_{11}H_{11}$ suggests interpretation as a spherical aromatic system with 32 core electrons in a filled $1S^21P^61D^{10}1F^{14}$ shell. The bare Ni, Pd, Pt metallaboranes studied here reinforce a fundamental principle: the geometry and electron-counting rules of boranes are so robust that even when a vertex is a transition metal with no external ligands, the cluster can remain intact and follow the same Wade–Mingos $2n + 2$ skeletal electron rule, gaining extra stability from three-dimensional aromaticity. This expands our understanding of cluster chemical space and hints at the possibility of isolating new types of molecules, namely metallaborane clusters that are ligand-free and aromatic.

Conflicts of interest

The authors have no conflict of interest to declare.

Data availability

Data are available from Prof. Alexandru Lupan upon request.

Supplementary information (SI): initial starting structures; distance matrices and energy rankings for the lowest energy structures; frontier molecular orbitals and their energies for the lowest energy $MB_{11}H_{11}$ structures; orbital energies and HOMO–LUMO gaps for the lowest energy structures. A concatenated

.xyz file containing the Cartesian coordinates of the optimized structures. See DOI: https://doi.org/10.1039/d5cp04106f.

Acknowledgements

This work was supported by a grant of the Ministry of Education and Research of Romania, CCCDI – UEFISCDI, project number PN-IV-PCB-RO-MD-2024-0515, within PNCDI IV. The computational resources were provided by the Babeş-Bolyai University under project POC/398/1/1/124155 – co-financed by the European Regional Development Fund (ERDF) through the Competitiveness Operational Program for Romania 2014–2020.

References

1 K. P. Callahan and M. F. Hawthorne, Ten years of metallocarboranes, *Adv. Organomet. Chem.*, 1976, **14**, 145–186.
2 R. N. Grimes, Role of metals in borane clusters, *Acc. Chem. Res.*, 1983, **16**, 22–26.
3 R. E. Williams, Carboranes and boranes; polyhedra and polyhedral fragments, *Inorg. Chem.*, 1971, **10**, 210–214.
4 R. E. Williams, The polyborane, carborane, carbocation continuum: architectural patterns, *Chem. Rev.*, 1992, **92**, 177–207.
5 K. Wade, The structural significance of the number of skeletal bonding electron-pairs in carboranes, the higher boranes and borane anions, and various transition-metal carbonyl cluster compounds, *J. Chem. Soc. D: Chem. Commun.*, 1971, 792–793.
6 D. M. P. Mingos, A general theory for cluster and ring compounds of the main group and transition elements, *Nature Phys. Sci.*, 1972, **236**, 99–102.
7 D. M. P. Mingos, Polyhedral skeletal electron pair approach, *Acc. Chem. Res.*, 1984, **17**, 311–319.
8 J.-I. Aihara, Three-dimensional aromaticity of polyhedral boranes, *J. Am. Chem. Soc.*, 1978, **100**, 3339–3342.
9 R. B. King and D. H. Rouvray, A graph-theoretical interpretation of the bonding topology in polyhedral boranes, carboranes, and metal clusters, *J. Am. Chem. Soc.*, 1977, **99**, 7834–7840.
10 R. B. King, Three-dimensional aromaticity in polyhedral boranes and related molecules, *Chem. Rev.*, 2001, **101**, 1119–1152.
11 A. Burke, D. Ellis, B. T. Giles, B. E. Hodson, S. A. Macgregor, G. M. Rosair and A. J. Welch, Beyond the icosahedron: the first 13-vertex carborane, *Angew. Chem., Int. Ed.*, 2003, **42**, 225–228.
12 L. Deng, H.-S. Chen and Z. Xie, Synthesis, structure, and reactivity of 13-vertex carboranes and 14-vertex metallacarboranes, *J. Am. Chem. Soc.*, 2006, **128**, 5219–5230.
13 W.-Y. Liang, J. Barroso, S. Jalife, M. Orozco-Ic, X. Zárate, X. Dong, Z. Cui and G. Merino, $B_{10}M_2$ (Rh, Ir): a stable boron-based icosahedral cluster, *Chem. Commun.*, 2019, **55**, 7490–7493.
14 D. Olaide-López, P. L. Rodriguez-Kessler, S. Rodriguez-Carrera and A. Muñoz-Castro, Hydrogen storage properties for bimetallic doped boron clusters M2B7 (M = Fe, Co, Ni), *Int. J. of Hydrogen Energy*, 2025, **107**, 419–425.
15 W. B. Schneider, G. Bistoni, M. Sparta, M. Saitow, C. Riplinger, A. A. Auer and F. Neese, Decomposition of intermolecular interaction energies within the local pair natural orbital coupled cluster framework, *J. Chem. Theory Comput.*, 2016, **12**, 4778–4792.
16 C. Riplinger, P. Pinski, U. Becker, E. F. Valeev and F. Neese, Sparse maps-A systematic infrastructure for reduced-scaling electronic structure methods. II. Linear scaling domain-based pair natural orbital coupled cluster theory, *J. Chem. Phys.*, 2016, **144**, 24109.
17 F. Pavosevic, P. Pinski, C. Riplinger, F. Neese and E. F. Valeev, SparseMaps-A systematic infrastructure for reduced-scaling electronic structure methods. IV. Linear-scaling second-order explicitly correlated energy with pair natural orbitals, *J. Chem. Phys.*, 2016, **144**, 144109.
18 A. Kubas, D. Berger, H. Oberhofer, D. Maganas, K. Reuter and F. Neese, Surface adsorption energetics studied with gold standard wave function-based ab initio methods: small-molecule binding to TiO_2(110), *J. Phys. Chem. Lett.*, 2016, **7**, 4207–4212.
19 M. Isegawa, F. Neese and D. A. Pantazis, Ionization energies and aqueous redox potentials of organic molecules: comparison of DFT, Correlated ab initio theory and pair natural orbital approaches, *J. Chem. Theory Comput.*, 2016, **12**, 2272–2284.
20 Y. Guo, K. Sivalingam, E. F. Valeev and F. Neese, parseMaps-A systematic infrastructure for reduced scaling electronic structure methods. III. Linear-scaling multireference domain-based pair natural orbital N-electron valence perturbation theory, *J. Chem. Phys.*, 2016, **144**, 94111.
21 A. K. Dutta, F. Neese and R. Izsak, Towards a pair natural orbital coupled cluster method for excited states, *J. Chem. Phys.*, 2016, **145**, 34102.
22 D. Datta, S. Kossmann and F. Neese, Analytic energy derivatives for the calculation of the first-order molecular properties using the domain-based local pair-natural orbital coupled-cluster theory, *J. Chem. Phys.*, 2016, **145**, 114101.
23 P. Pinski, C. Riplinger, E. F. Valeev and F. Neese, Sparse maps-A systematic infrastructure for reduced scaling electronic structure methods. I. An efficient and simple linear scaling local MP2 method that uses an intermediate basis of pair natural orbitals, *J. Chem. Phys.*, 2016, **143**, 34108.
24 B. Mondal, F. Neese and S. F. Ye, Control in the rate-determining step provides a promising strategy to develop new catalysts for CO_2 Hydrogenation: A local pair natural orbital coupled cluster theory study, *Inorg. Chem.*, 2015, **54**, 7192–7198.
25 D. G. Liakos, M. Sparta, M. K. Kesharwani, J. M. L. Martin and F. Neese, Exploring the accuracy limits of local pair natural orbital coupled-cluster theory, *J. Chem. Theory Comput.*, 2015, **11**, 1525–1539.

26 D. G. Liakos and F. Neese, Domain based pair natural orbital coupled cluster studies on linear and folded alkane chains, *J. Chem. Theory Comput.*, 2015, **11**, 2137–2143.
27 D. G. Liakos and F. Neese, Is it possible to obtain coupled cluster quality energies at near density functional theory cost? Domain-based local pair natural orbital coupled cluster vs modern density functional theory, *J. Chem. Theory Comput.*, 2015, **11**, 4054–4063.
28 O. Demel, J. Pittner and F. Neese, A local pair natural orbital-based multireference Mukherjee's coupled cluster method, *J. Chem. Theory Comput.*, 2015, **11**, 3104–3114.
29 Y.-F. Shen, C. Xu and L.-J. Cheng, Chemical bonding in $B_nH_n^{2-}$, AdNDP analysis of *closo* boranes, *RSC Adv.*, 2017, **7**, 36755–36764.
30 Gaussian09 (Revision E.01), Gaussian, Inc., Wallingford, CT, 2009. The complete reference is given in the SI.
31 F. Neese, The ORCA program system, *Wiley Interdiscip. Rev.: Comput. Mol. Sci.*, 2012, **2**, 73.
32 R. IzsIak and F. Neese, Speeding up spin-component-scaled third-order pertubation theory with the chain of spheres approximation: the COSX-SCS-MP3 method, *Mol. Phys.*, 2013, **111**, 1190.
33 R. IzsIak and F. Neese, An overlap fitted chain of spheres exchange method, *J. Chem. Phys.*, 2011, **135**, 144105.
34 S. Kossmann and F. Neese, Efficient structure optimization with second-order many-body perturbation theory: The RIJCOSX-MP2 method, *J. Chem. Theory Comput.*, 2010, **6**, 2325–2338.
35 S. Kossmann and F. Neese, Comparison of two efficient approximate Hartree-Fock approaches, *Chem. Phys. Lett.*, 2009, **481**, 240–243.
36 F. Neese, F. Wennmohs, A. Hansen and U. Becker, Efficient, approximate and parallel Hartree-Fock and hybrid DFT calculations. A chain-of-spheres algorithm for the Hartree-Fock exchange, *Chem. Phys.*, 2009, **356**, 98–109.
37 F. Neese, An improvement of the resolution of the identity approximation for the calculation of the Coulomb matrix, *J. Comput. Chem.*, 2003, **24**, 1740–1747.
38 A. K. Dutta, F. Neese and R. Izsak, Speeding up equation of motion coupled cluster theory with the chain of spheres approximation, *J. Chem. Phys.*, 2016, **144**, 34102.
39 G. J. Christian, F. Neese and S. F. Ye, Unravelling the molecular origin of the regiospecificity in extradiol catechol dioxygenases, *Inorg. Chem.*, 2016, **55**, 3853–3864.
40 E. D. Jemmis and P. v R. Schleyer, Aromaticity in three dimensions. 4. Influence of orbital compatibility on the geometry and stability of capped annulene rings with six interstitial electrons, *J. Am. Chem. Soc.*, 1982, **104**, 4781–4788.
41 A. Hirsch, Z. Chen and H. Jiao, Spherical aromaticity in I_h symmetrical fullerenes: The $2(N + 1)^2$ rule, *Angew. Chem.*, 2000, **39**, 3915–3917.